JREE: Vol. 11, No. 2, (Spring 2024) 58-66

Journal of Renewable Energy and Environment

Journal Homepage: www.jree.ir

Materials and Energy Research Center

MERC

Research Article

Improving the Energy Performance of an Evacuated Tube Solar Collector Water Heater Using Compound Parabolic Concentrator: an Experimental Study

Mahdi Pourbafrani [a], Hossein Ghadamian [a,*], Mohammad Aminy [a], Meisam Moghadasi [a], Masoud Mardani [a], Mohammad Akrami [b], Amir Houshang Khaki [c], Seyed Mohammad Kazem Sadr [b,c]

[a] Department of Energy, Materials and Energy Research Center, Karaj, Iran.
[b] Department of Engineering, University of Exeter, Exeter, UK.
[c] Department of Research & Development, Chamberlains Aqua Systems Limited, Southampton, UK.

PAPER INFO

Paper History:
Received: 10 November 2023
Revised: 08 February 2024
Accepted: 12 March 2024

Keywords:
Vacuum Tube Solar Water Heater,
Evacuated Tube Solar Collector,
Central Parabolic Concentrator,
Energy Performance,
Experimental Investigation

ABSTRACT

Evacuated tube solar collectors (ETSC) are widely utilized in both domestic and industrial solar water heaters (SWH) due to their commendable thermal performance and straightforward installation. However, a significant challenge associated with ETSC lies in the fact that half of the collector remains unexposed to sunlight. To overcome this limitation, parabolic reflectors can be employed as a viable solution. The primary objective of this study is to assess the performance of a compound parabolic concentrator (CPC) in conjunction with ETSC, taking into account a specific ratio between the areas of the CPC and ETSC. To achieve the desired configuration, the CPC was meticulously designed, fabricated, installed, and subsequently tested. Moreover, the energy performance of the absorber tube was scrutinized both with and without the integration of a parabolic trough collector. The experiments and data collection were conducted on two selected days for both the conventional ETSC device and the system incorporating the CPC. Meteorological data and operational conditions were measured and digitally stored for subsequent analysis. A noteworthy outcome of the study is the revelation that the energy efficiency of the system with a concentrator exhibited a notable improvement of 2.8% compared to the conventional system. Offline results further indicated that the performance of a single absorber tube with a concentrator increased by approximately 2.7 times when compared to the standard system. This suggests that the energy performance of the solar water heater, with a capacity of about 200 liters and featuring 7 absorber tubes with a concentrator, is comparable to that of the conventional system equipped with 18 absorber tubes.

https://doi.org/10.30501/jree.2024.424000.1728

1. INTRODUCTION

The global demand for energy has seen steady growth with the increasing population, technological advancements, and industrial expansion (Ghadamian et al., 2024). Addressing this challenge is crucial, and renewable energy resources, particularly solar energy, are recognized as a key solution (Moghadasi et al., 2023). Solar systems, especially Evacuated Tube Solar Collectors (ETSC), have been widely implemented in both industries and homes in recent years (Qiu, Ruth and Ghosh, 2015). ETSC systems exhibit efficient performance at high temperatures, attributed to tube evacuation preventing convection and conduction losses. This feature makes them highly preferable for specific applications like desalination or absorption cooling systems requiring high-temperature thermal energy (Budihardjo and Morrison, 2009). Additionally, ETSC systems are acknowledged as a prominent method for utilizing solar thermal energy (Mevada et al., 2022) and present an energy-saving opportunity for effective energy management (Moghadasi et al., 2021). In a study by Sadeghi, Safarzadeh, and Ameri (2019), various methods were explored to enhance the thermal efficiency of an ETSC, including the addition of a flat reflector, a parabolic concentrator, and the utilization of a nanofluid. The focus was on nanofluids, specifically Cu_2O soluble in water, with a volume ratio ranging from 0.01 to 0.08%. Results showed that the energy and exergy efficiencies improved significantly when nanofluid with a concentration of 0.08% and a parabolic concentrator were employed. Teles, Ismail, and Arabkoohsar (2019) investigated the incorporation of a reflector in the inner layer of the outer tube in the ETSC system. Their modeled system achieved efficiency levels ranging from approximately 73% to 42%. Xia and Chen (2020) examined the thermal performance of systems combining multiple ETSCs and mini-CPCs. Using a unique design, a shortened CPC positioned between vacuum tubes resulted in an increased water temperature of 13.6 °C compared to the device

*Corresponding Author's Email: h.ghadamian@merc.ac.ir (H.Ghadamian)
URL: https://www.jree.ir/article_193274.html

Please cite this article as: Pourbafrani, M., Ghadamian, H., Aminy, M., Moghadasi, M., Mardani, M., Akrami, M., Khaki, A. H. & Sadr, S. M. K. (2024). Improving the Energy Performance of an Evacuated Tube Solar Collector Water Heater Using Compound Parabolic Concentrator: an Experimental Study, *Journal of Renewable Energy and Environment (JREE)*, 11(2), 58-66. https://doi.org/10.30501/jree.2024.424000.1728.

without the mini-CPC. Li et al. (2020) analyzed the efficiency of a double-row all-glass evacuated tube SWH, considering different pipes' declination angles. The highest energy efficiency, observed at a 2-degree declination angle, reached 74.1%. Kumar and Mylsamy (2020) studied the effect of Nano-Enhanced Phase Change Materials (NEPCMs), particularly nano-CeO_2, on ETSC performance. Optimal performance was achieved with a nanoparticle mixture in the water heater tank, resulting in energy and exergy efficiencies of 79.2% and 8.59%, respectively. Fathabadi (2020) investigated the performance of a single evacuated tube using single- and dual-axis reflectors and trackers. The system with a reflector and biaxial tracker achieved a thermal efficiency of 58.60%, presenting technical feasibility but limited economic viability. Sasikumar et al. (2020) analyzed the effect of utilizing Al_2O_3 nanofluid on ETSC system performance. At a concentration of 0.3% by volume, the system reached its peak performance of 69.5%, focusing solely on nanofluid as a means to enhance efficiency. Deng and Chen (2020) conducted an analysis of the efficiency of a single-pipe EBIETC system under real conditions. The results from the experimental tests revealed that the highest and average thermal efficiencies of the EBIETC were 55.4% and 51.4%, respectively. While the concept of incorporating pipes into the building's walls is innovative, certain operational and financial limitations exist. Moreover, Ismail, Teles, and Lino (2021) delved into the efficiency of an evacuated tube with an off-center inner tube, comparing circular and rectangular absorbers using Al_2O_3 nanofluid. Simulating the vacuum tube's performance demonstrated that the circular absorber exhibited an 8% efficiency, outperforming the rectangular absorber. Considering nanofluids with a volume ratio ranging from 0.01 to 0.1, the maximum efficiency of 8.8% was achieved using a circular absorber.

Additionally, Chai et al. (2021) proposed, tested, and analyzed the performance of an ETSC-IC through experimental investigations in 2021. Examination of the light reflection conditions revealed that the optimal evacuated tube cover angle is 180 degrees. The ETSC-IC system achieved its highest efficiency at approximately 72%. While this research demonstrates creativity in terms of reflective utilization, it involves modifying the structure of the ETSC and introduces significant technical complexities. In a separate study, Chen and Liu (2022) undertook a redesign of the M-CPC to enhance the optical performance of a vacuum tube. They proposed five different designs for the multi-part parabolic concentrator, utilizing two algorithms: Particle Swarm Optimization and Monte Carlo Ray Tracing. Among the designs, M-CPC5 achieved the highest performance, boasting a maximum optical efficiency of 61.68%. However, it should be noted that the study exclusively reports the optical efficiency. Additionally, in the work by Chen, Yang, and Li (2022), modifications were made to the placement angle of the collectors, and a flat reflector was incorporated to enhance the thermal power of ETSC systems during the cold season. This research aims to tackle the issue of reduced efficiency during winter and overheating in the summer, which are commonly observed challenges in these systems. According to the measurement results, the device's performance increased by 66% in December but decreased by 66% in June. Details of the relevant studies are presented in Table 1.

Table 1. Detailed description of related works

Author(s) / year	Method of SWH performance analysis	Main findings
Sadeghi, Safarzadeh, and Ameri (2019)	The effects of using a flat reflector, a parabolic concentrator, as well as the use of nanofluid, on the thermal efficiency of the ETSC water heater were experimentally investigated.	By employing a parabolic concentrator and nanofluid, the maximum thermal efficiency of 78% was obtained.
Teles, Ismail, and Arabkoohsar (2019)	Utilizing a reflector in the inner layer of an evacuated tube to improve thermal efficiency.	The maximum theoretical thermal efficiency of 73% was achieved by installing a reflector inside the tube.
Xia and Chen (2020)	The effects of employing shortened CPC were experimentally investigated on the thermal efficiency of an ETSC.	The thermal efficiency increased from 29.2% to 24.3%.
Li et al. (2020)	The effect of changing the middle angle in the horizontal double-row ETSC water heater on thermal efficiency was investigated through experimentation.	The maximum thermal efficiency of 74.1% was obtained.
Kumar and Mylsamy (2020)	The effect of phase change materials on the thermal performance of an ETSC water heater was analyzed.	The maximum efficiency was achieved at 79.2% using phase-change materials.
Fathabadi (2020)	The effects of using a reflector and one and two-axis trackers on the thermal efficiency of an ETSC were experimentally evaluated.	The maximum thermal efficiency reached 58.60% in the economical optimum mode applying a reflector and two-axis tracker.
Sasikumar et al. (2020)	The effects of using nanofluid on the thermal performance of an ETSC water heater were experimentally investigated.	The maximum thermal efficiency using nanofluid was 69.5%.
Deng and Chen (2020)	The effects of using a redesigned CPC on the thermal efficiency of an ETSC installed in the building wall were experimentally assessed.	Through this shortened CPC, the maximum thermal efficiency was achieved at 55.5%.
Ismail, Teles, and Lino (2021)	The effects of using nanofluid and changing the cross-sectional shape of the vacuum tube with an internal absorber tube in the thermal performance of an ETSC were numerically examined.	The maximum thermal efficiency improvement using nanofluid was obtained by the circular cross-section of the internal absorber tube of 8.8%.
Chai et al. (2021)	The idea of using a reflector in the inner layer of a vacuum tube to improve thermal efficiency was experimentally investigated.	The experimental thermal efficiency value was improved by 10% employing a reflector inside the tube.
Chen and Liu (2022)	The effects of using the optimal CPC designed with the PSO and MCRT algorithms on the optical efficiency of an ETSC were experimentally studied.	The maximum optical efficiency was 61.68% using this shortened CPC.
Chen, Yang and Li (2022)	The effects of changing the angle and reflector on the thermal efficiency of an ETSC water heater were experimentally studied.	The experimental thermal efficiency value in December improved by 66% by changing the angle and installing the reflector.

In the field of concentrators, previous research has made efforts to enhance efficiency. However, the clarity of geometry and relevant physical data is not consistently maintained. The primary goal of this study is to elucidate the effects contributed by reflectors, irrespective of the nanofluid application. Achieving this objective necessitates the development of a new pattern and shape to overcome existing obstacles. To fill the mentioned gaps, the following tasks will be undertaken in detail:

- In a detailed experimental study, the ratio of the concentrator area to the ETSC area will be investigated.
- The effect of using a parabolic concentrator on thermal performance will be examined.
- The change in solar energy absorption rate for the entire solar water heater and ETSC will be analyzed.

This paper investigates the thermal performance and the change in solar energy absorption rate of an Evacuated Tube Solar Collector (ETSC) after the installation of a simple parabolic concentrator. This will be achieved by adding a portion of the concentrator area, in comparison to the nominal area of the absorber. To provide a novel comparison tool, the performance of the Solar Water Heater (SWH) has been evaluated using a new coefficient, denoted as *"α"*, representing the absorption rate of solar energy required to increase the temperature of 1 kg of working fluid by 1°C. Furthermore, in this research, the coefficient α is employed as another innovative measure to explore the possibility of reducing the number of ETSCs while maintaining the same overall absorbed heat energy value. This reduction is made possible by replacing the vacuum tubes with a parabolic concentrator, resulting in improved energy performance.

2. MATERIALS AND METHODS

2.1. SWH System Description

The proposed SWH system comprises 18 ETSCs utilizing a passive circulation cycle, complemented by a parabolic concentrator for the central absorber tube, as illustrated in Figure 1.

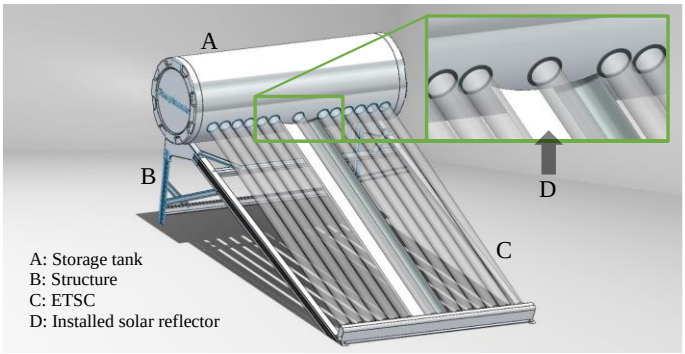

Figure 1. Overview of the proposed scheme

The SWH operates as a non-pressure type. Municipal water, serving as the working fluid, is in direct contact with the absorber vacuum tubes, allowing it to receive the absorbed radiation energy directly. The chamber between two absorber glasses is vacuumed and coated to increase energy efficiency and energy absorption rate (Chen, Xia and Bie, 2019). The vacuum tubes absorb sunlight during the day and transfer energy to the working fluid, thereby increasing its temperature (Milani and Abbas, 2016). In this cycle, the hot water moves up through the thermosiphon phenomenon. Due to temperature differences, the water inside the storage tank replaces the water in the vacuum tubes. The parabolic concentrator aids in increasing the energy received by the central absorber tube by converging the radiation rays that pass around it (Wang et al., 2021).

2.2. System Design

Since there is a gap between the central absorber tubes, a symmetrical CPC in a partial circle shape is required to redirect the transmitted radiation from the empty gap to the surface of the absorber tube. To focus the reflected radiation, as shown in Figure 2, the vacuum absorber tube is positioned at the focal point of the CPC. The design of this concentrator is based on the space behind the absorber tube (d) and assuming a certain angle φ. The radius of the imaginary circle r is expressed as (Chen, Xia and Bie, 2019):

$$r = \frac{d}{2\,sin\frac{\varphi}{2}} \quad (1)$$

After determining r, the arc length of the concentrator R as well as the focal distance F of the concentrator can be calculated as follows:

$$R = 2\pi r \frac{\varphi}{360} \quad (2)$$

$$F = \frac{r}{2} \quad (3)$$

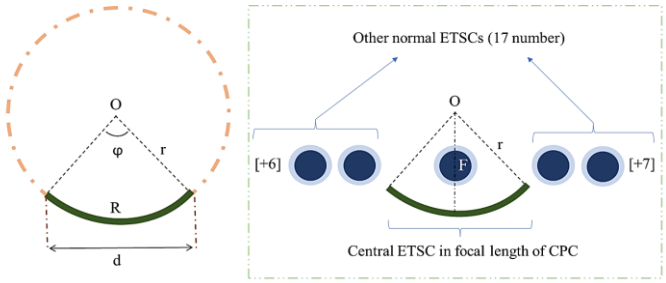

(a) (b)

Figure 2. (a) The details of the concentrator design. (b) the bottom view of the concentrator placement on the central absorber and the arrangement of the absorber tubes.

2.3. Experimental Set-up

The tested SWH has overall dimensions of 1740×1650×1500 mm (Figure 3) and consists of 18 symmetrical ETSCs with a length of 1800 mm for solar radiation absorption. It features a cylindrical water storage tank with a capacity of 142 liters, positioned on top of the SWH and insulated by a 50 mm thick foam layer. The vacuum absorber tubes are connected to the tank using O-rings. Each vacuum absorber tube has a water storage capacity of 3 liters, resulting in a total capacity of 54 liters for the 18 absorber tubes, and the system has a total capacity of 196 liters. An assistant tank is situated above the storage tank and is connected to the inlet water through a float valve (ballcock) to compensate for water evaporation in the main tank (Chai et al. 2021). The specifications of the proposed system are provided in Table 2.

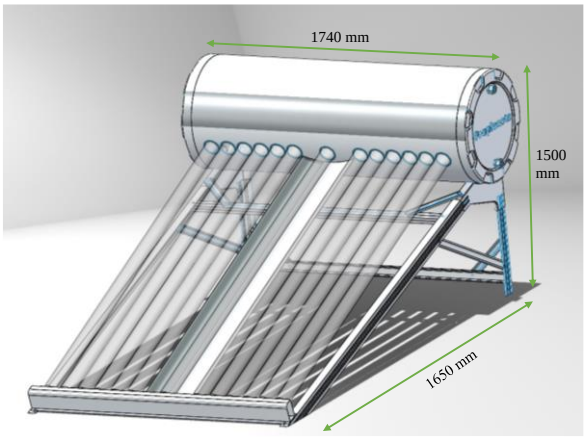

Figure 3. Sizing diagram of the experimental setup

Table 2. System specifications (Chai et al. 2021)

No.	Specification	Value/type
1	Evacuated tube outer layer material	Borosilicate glass
2	Evacuated tube length	1800 mm
3	Evacuated tube outer diameter	58 mm
4	Evacuated tube inner diameter	47 mm
5	Evacuated tube inner coating material	Al-Nickel
6	Evacuated tube emissivity	0.88
7	Evacuated tube transmissivity	0.94
8	Evacuated tube volume	3 (Liters)
9	Number of evacuated tubes	18
10	Total Evacuated tubes volume	54 (Liters)
11	Storage tank material	Grade 304 stainless steel
12	Storage tank volume	142 (Liters)
13	Storage tank insulation material	50 mm polyurethane foam
14	Structure material	Galvanized steel frame
15	Total SWH volume	196 (Liters)

2.4. Measurements Instruments

In this research, a local meteorological station and a data logger were developed and constructed to accurately measure and record relevant variables. The meteorological station was designed to assess ambient temperature, wind velocity, and solar radiation intensity. Simultaneously, the data logger, equipped with temperature sensors, stored the functional characteristics of the system. These sensors played a crucial role in monitoring the temperature of the water flow during the thermosiphon inside the pipe. For temperature measurement, one sensor was strategically placed in the path of the hot return flow from the absorber tube, while another sensor was positioned in the path of the cold flow from the tank. Additionally, a sensor at the center of the storage tank was employed to measure the water temperature within the tank. An anemometer of the Robinson 4 Cups type was positioned under the absorber tubes to accurately measure wind velocity as air passed through them. To gauge solar irradiance, a pyranometer was installed between the absorber and parallel tubes. The data logger efficiently recorded the values of all sensors simultaneously at 30-second intervals, as detailed by Pourbafrani et al. (2023). Table 3 provides specifications for the sensors used in the study. For a visual representation, refer to Figure 4, which illustrates the specific locations of the sensors.

Table 3. The detailed specifications of the instruments

No.	Instrument/Model	Application	Range	Accuracy
1	Digital RTD thermometer / PT100	Measuring air and water temperatures	0 – 120 °C	±0.1 °C
2	Anemometer / 652-1010	Measurement of wind speed	0 – 30 m/s	±0.3 m/s
3	Ambient lux meter / BH1750	Measuring solar irradiance	0 – 1200 W/m^2	±2 %

2.5. Experimental Procedure

The experiment was conducted in Karaj city, Iran, situated at a latitude of 35.74 and a longitude of 50.95, during the month of July (summer case). The device was fixed in position, oriented towards the geographical south at an angle of 45 degrees, without the use of a *tracker*. Prior to each test and sunrise, the system tank was filled with municipal water at the same temperature as the surrounding environment. six parameters were measured, stored, and subsequently used for further analysis. Following each data collection session, the hot water in the tank was utilized, and the tank was refilled with cold water before sunrise. Importantly, no modifications were made to the system or the water in the storage tank throughout the data collection period. Furthermore, the Durbin-Watson statistics method was applied for uncertainty analysis (refer to Section 2.9).

Table 4. Description of the attributes

No.	Variable	Abbreviation	Unit	Interval
1	Temperature of hot water exit from thermosiphon cycle	T_h	°C	11:30 – 16:30, Every 30 s
2	Temperature of cold water enters in thermosiphon cycle	T_c	°C	
3	Temperature of tank	T_t	°C	
4	Temperature of air	T_a	°C	
5	Wind speed	v	m/s	
6	Solar irradiance	G_s	W/m^2	

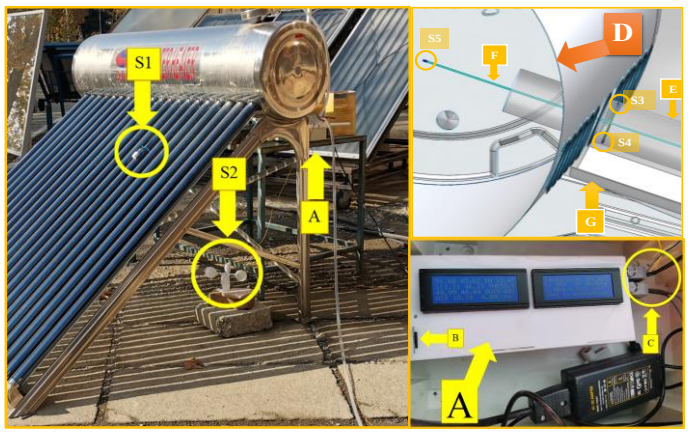

Figure 4. A) Data logger and components, B) SD card slot, C) Sensors connectors, D) Cross section of a storage tank, E) Central ETSC with temperature sensors, F) Sensor's stand, G) Installed CPC under central ETSC, S1) Ambient light sensor for measuring G_S, S2) anemometer, S3&S4) PT100 temperature sensor installed in a special stand (E) Place for insert sensor into the central ETSC, S5) Storage tank temperature sensor (T_t)

2.6. Energy Performance of SWH

In the case of this particular Solar Water Heater (SWH) type, it is assumed that the density, specific heat, and volume of water remain constant during the test period. This assumption is based on the non-change of the water phase in the storage tank. As a result, the energy absorbed by the SWH can be determined using Equation 4 (Chen, Xia and Bie, 2019):

$$Q_{use} = \frac{2\times\pi\times\lambda_{gl}\times L\times(T_{io}-T_{ii})}{ln\,(\frac{D_{io}}{D_{ii}})} = \pi \times D_{ii} \times L \times h_w \times (T_{ii} - T_w) \quad (4)$$

where Q_{use} = useful energy, λ_{gl} = thermal conductivity of glass, L = tube length, T_{io} = outer temperature of the inner tube, T_{ii} = internal temperature of the inner tube, D_{io} = outer diameter of the inner tube, D_{ii} = internal diameter of the inner tube, and T_w = working fluid temperature. The water temperature (T_w) is the average of integrated values based on a period of data:

$$T_w = (T_{w,st} + T_{w,e})/2 \quad (4.1)$$

$$h_w = \frac{Nu_w\times D_{ii}}{\lambda_w} \quad (4.2)$$

where $T_{w,st}$, $T_{w,st}$, and λ_w denote the working fluid temperature at the beginning of the period, working fluid temperature at the end of the period, and thermal conductivity of water, respectively. The modified Nusselt number would be calculated based on the following equations:

$$Nu_{fl} = 0.82 \times C_o \times [Pr_w \times \frac{g\times Q_w\times D_{ii}^4\times\gamma_w}{A_{ii}\times\lambda_w\times\nu_w^2} \times \left(\frac{L}{D_{ii}}\right)^{3.4}]^{0.2} \quad (4.3)$$

$$C_o = 4.3324sin^4\beta + 6.9312sin^3\beta - 4.6872sin^2\beta + 1.1827sin\beta + 1.0007 \quad (4.4)$$

where C_o = correction factor of Nusselt number, A_{ii} = internal area of the inner tube, and β = collector inclination angle. The physical properties of water including thermal conductivity (λ_w), specific weight (γ_w), kinematic viscosity (ν_w), and Prandtl number (Pr_w) are obtained by the interpolation method using T_w. In addition, the total solar radiation received on SWH absorbers and the energy efficiency of SWH are calculated using the following formulas (Moghadasi et al., 2022):

$$Q_{in} = G_s * A_{abs} \quad (5)$$

$$\eta_{en} = \frac{Q_{use}}{Q_{in}} \quad (6)$$

where A_{abs} = absorber cross-sectional area and G_s = solar irradiation.

2.7. Exergy Efficiency of SWH

Neglecting the volume changes of water in the tank, the system exergy changes in the initial and the final state of the SWH measurement period are as follows (Khanmohammadi et al., 2020):

$$Ex_{st} = m_w \times C_{P,w} \times [T_{t,st} - T_0 \times \left(1 + ln\,(\frac{T_{t,st}}{T_0})\right)] \quad (7)$$

$$Ex_e = m_w \times C_{P,w} \times [T_{t,e} - T_0 \times \left(1 + ln\,(\frac{T_{t,e}}{T_0})\right)] \quad (8)$$

where Ex_{st} = exergy at the beginning of the period, m_w = ware mass, $C_{p,w}$ = specific heat capacity of water, $T_{t,st}$ = storage tank temperature at the beginning of the period, $T_{t,e}$ = storage tank temperature at the end of the period, and Ex_e = exergy at the end of the period. Also, the exergy of received solar radiation in SWH is defined as follows (Khanmohammadi et al., 2020):

$$Ex_s = G_s \times A_{abs} \times [1 - \frac{4}{3}\left(\frac{T_a}{T_s}\right) + \frac{1}{3}\left(\frac{T_a}{T_s}\right)^4] \quad (9)$$

where T_s and T_a represent the sun's surface temperature and ambient temperature. Finally, the exergy efficiency of the system is obtained by dividing the exergy of the final state by the sum of the exergy of the received solar radiation and the exergy of the initial state (Khanmohammadi et al., 2020):

$$\eta_{ex} = \frac{Ex_e}{Ex_{st}+Ex_s} \quad (10)$$

2.8. Energy Absorption Rate of SWH and ETSC

The energy efficiency of the system is expressed as (FathiAlmas et al., 2023):

$$\eta_{en} = \frac{Q_{use}}{Q_{in}} = \frac{m_w\times C_{P,w}\times(T_{t,e}-T_{t,st})}{G_s\times A_{abs}} \quad (11)$$

By eliminating the specific heat capacity of water ($C_{P,w}$), absorber cross-sectional area (A_{abs}), and reversing the expression, a new index called "α" is obtained as follows:

$$\alpha_{SWH} = \frac{G_s}{m_w\times(T_{t,e}-T_{t,s})}\ (\frac{W}{m^2.kg.^\circ C}) \quad (12)$$

α represents the solar radiation required by SWH to raise the temperature of 1 kg of water by 1°C. α_{SWH} represents the radiation received by the solar water heater's ETSCs. Considering that all absorber tubes are identical, the value of α_{SWH} for an absorber tube can be obtained by dividing α_{SWH} by the total number of vacuum absorber tubes:

$$\bar{\alpha}_{ETSC} = \frac{\alpha_{SWH}}{n_{ETSC}} \quad (13)$$

$\bar{\alpha}_{ETSC}$ indicates the average radiation absorbed by each ETSC for 1°C of temperature increase from one kilogram of tank water.

2.9. Measurement Error Evaluation

It is imperative to conduct error analysis before delving into the examination of experimental test data. A frequently employed method for such analysis is the Autocorrelation test, carried out using the Durbin-Watson statistics method (Durbin and Watson, 1950). This test becomes particularly relevant when data has been gathered over a period of time. Autocorrelation manifests when a correlation exists between the residuals (errors) in one data interval and those in another interval (Durbin and Watson, 1971). The recommended interpretation for the value of this statistical parameter is as follows (Seidabadi et al., 2022):

$$\mathrm{DW} = \frac{\sum_{i=2}^{T}(e_i - e_{i-1})^2}{\sum_{i=1}^{T} e_i^2} \quad (14)$$

In the above equation, e_i represents the residual value in the i^{th} observation and n denotes the number of observations. The DW parameter can range between 0 and 4. Values between 0 and 2 indicate the possibility of a positive correlation, while values between 2 and 4 suggest the possibility of a negative correlation. In this study, the DW test was conducted using average values of the variables at 5-minute intervals.

3. RESULTS AND DISCUSSION

3.1. System Design

Based on the design procedure (refer to Section 2.2), the distance between the two tubes was calculated as d = 194 mm. Using Equation 1 and assuming φ = 51.42°, the approximate value of r was found to be 223 mm. By determining r and applying Equation 3, the focal distance of the convex concentrator was calculated as F = 111.5 mm. Also, Equation 2 was used to estimate the length of the arc, resulting in ≈ 200 mm. Accordingly, the concentrator was fabricated utilizing stainless steel, as shown in Figure 5. Additionally, the supporting structure, made of MDF, was designed and built to position the ETSC at the focal point of the concentrator. It should be noted that the area of the CPC is 0.3 m^2, while the surface area of an ETSC absorber is 0.24 m^2. Thus, the area of a CPC is 1.25 times larger than the surface area of the ETSC absorber.

(a) (b)

Figure 5. (a) ETSC after installing the parabolic concentrator; (b) experiment setup without the concentrator

3.2. Experimental Measurements Results

Since meteorological data and weather conditions are the primary influencing factors in the systems, it is crucial to ensure that environmental conditions are similar to increase the accuracy of comparing performance before and after the changes. To achieve this, data collection was conducted on two consecutive days: Day 1 (July 10) for the SWH without a concentrator and Day 2 (July 11) for the SWH with the installed concentrator. The aim was to have normal (stable, natural) and similar meteorological data and weather conditions for both days. The monitoring of the system started at 11:30 AM and continued until 4:30 PM. During this period, parameters such as solar irradiance, air temperature, and wind speed were measured at the test site. The measurement results for the two days indicated that the average radiation was 784 $\frac{W}{m^2}$ and 768 $\frac{W}{m^2}$, the average air temperatures were 36.80 ºC and 37.41 ºC, and the average wind speeds were 1.05 m/s and 0.83 m/s, respectively. These data provide an understanding of the prevailing conditions during the experimental period.

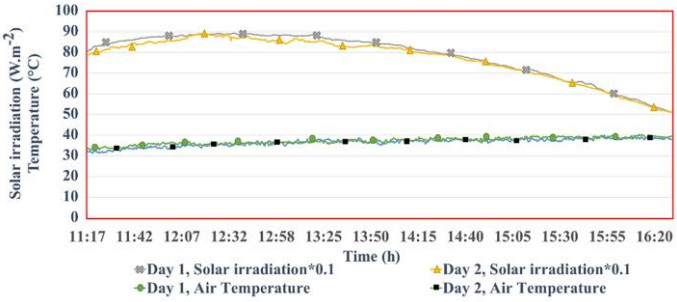

Figure 6. Comparison of **changes** in radiation and air temperature during two different data collection periods

Figure 6 demonstrates that weather conditions were similar on the two test days. The calculations were performed step by step at 30-second intervals, allowing for a detailed analysis of the overall energy balance, including input energy, useful shares, and losses. The initial data, which comprises system start-up information and meteorological conditions, is monitored and used as input data at time t = 0. Based on the physical characteristics of the SWH and the model calculations, the tank temperature is determined. This temperature serves as a variable representing the dynamic behavior of the system and can be compared between the experimental and theoretical models. To solve the models, an open-source program called Quick-Basic is developed, employing a trial-and-error objective function. The average difference percentage between theory and experiments is found to be 0.8% on Day 1 (July 10) and 0.7% on Day 2 (July 11), indicating a good agreement between the experimental and theoretical models. In 2019, Chen, Xia, and Bie presented the experimental results along with the heat transfer and physical models. These results are depicted in Figure 7 as dotted lines, which are compared with the experimental data obtained in this research.

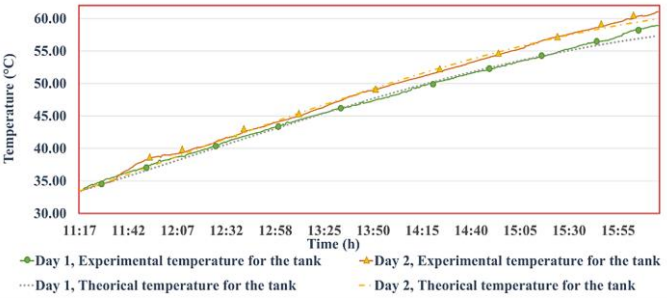

Figure 7. Comparison of tank temperature changes with theory and experiments in Day 1 and Day 2

According to Figure 7, at the start of the system monitoring, the temperature of the tank was 33.4 ºC in both cases. By the end of the test period, the water temperature in the regular system reached 58.89 ºC, while in the system with the concentrator, it reached 61.29 ºC. Therefore, there was an increase of 2.35 ºC compared to the normal system without the concentrator. Table 5 provides the measured value range for both the regular device and the system with the CPC to describe the measurement results.

Table 5. The range of measured data

No.	Variable (Unit)	System without the CPC (on Day 1)			System with the CPC (on Day 2)		
		Min.	Max.	Mean	Min.	Max.	Mean
1	G_s (W/m^2)	510.77	893.35	784.57	489.65	819.92	770.22
2	T_a (℃)	31.96	39.97	36.80	33.36	40.34	37.40
3	T_t (℃)	33.41	58.93	46.99	33.45	61.11	48.28
4	v (m/s)	0.00	5.50	1.05	0.00	4.95	0.83
5	T_h (℃)	22.62	49.61	36.32	27.75	53.54	40.37
6	T_c (℃)	23.56	47.35	37.19	25.40	47.23	36.88

3.3. Measurement Error Analysis

Using the Durbin-Watson table (King, 1992), the following values were considered to specify d_L and d_U: (a) significance level = 0.05; (b) k = 4; (c) n = 60. Accordingly, the values were found as d_L=1.444 and d_U=1.727. The test results for six attributes are shown in Figure 8.

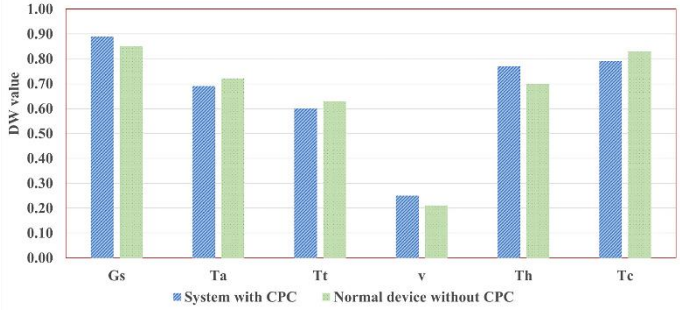

Figure 8. DW test results

Based on the calculation results and Figure 8, the DW test values of the variables were less than d_L, and, thus, the autocorrelation issue was not detected. Hence, the collected data were reliable and could be used for further analysis.

3.4. SWH Energy and Exergy Efficiencies Analysis

This section has investigated the effect of increasing the received radiation using CPC on the thermal performance of the system. During the test period, energy and exergy efficiencies have been compared at one-hour intervals, as displayed in Figure 9.

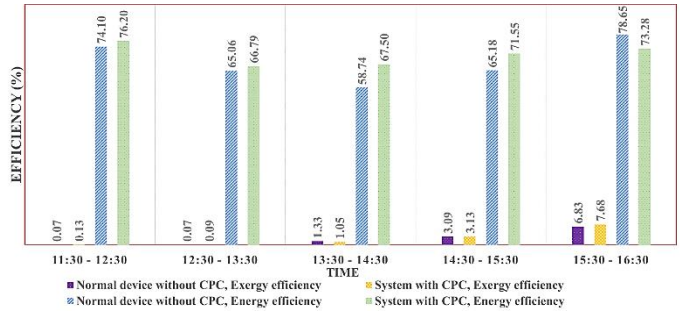

Figure 9. Comparison of energy and exergy efficiencies of the normal device and system with CPC in different time intervals

According to Figure 9, the average thermal efficiency of the conventional device and the system with the concentrator was 68.3% and 71.1%, respectively. This represents a 2.8% increase in energy efficiency when the concentrator is used. The average exergy efficiencies for the conventional device and the system with CPC were 2.28% and 2.42%, respectively. In addition, the performance curve equations are presented in Figure 10 and Table 6, which results from fitting the curve on the experimental data collected from continuous data collection on two different days.

Table 6. The proposed performance curve equations in the present work.

Experimental setup	Performance curve equation
With CPC	$\eta_i = 0.747 - 1.50\frac{(T_w - T_a)}{G_s}$
Without CPC	$\eta_i = 0.729 - 2.75\frac{(T_w - T_a)}{G_s}$

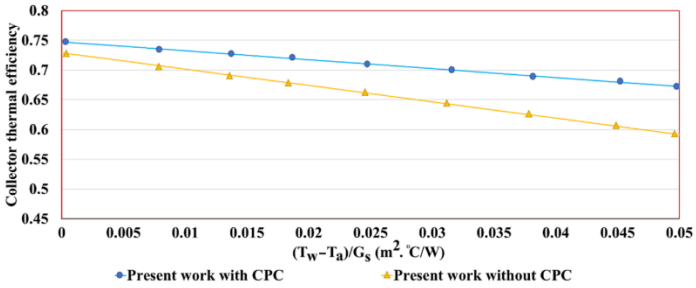

Figure 10. Comparison of the equations of the efficiency change curve of the proposed system

The slope of the curve in Figure 10 represents the heat loss coefficient parameter. As shown in Figure 10, after installing the CPC, the slope of the curve is lower than the case without CPC. This indicates that the proposed system has a lower heat loss coefficient than the conventional device.

3.5. Net Energy Absorption Rate Analysis

In addition to energy and exergy efficiencies, the performance analysis of the proposed system was also conducted using the coefficient of α in different time intervals, as depicted in Figure 11.

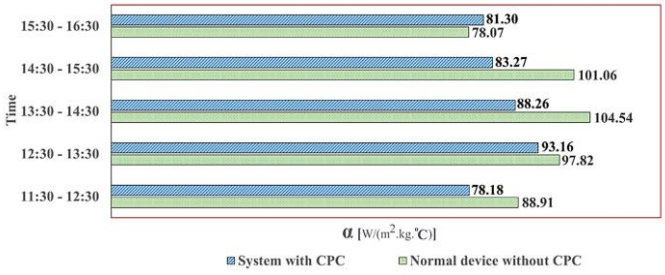

Figure 11. Comparison of α in different time intervals

According to Figure 11 and the calculated results, the SWH with 18 vacuum absorber tubes without concentrator required an average of 94.08 $\frac{W}{m^2}$ of solar energy flux to increase the temperature of 1 kg of tank water by 1°C, resulting in $\alpha_{SWH,normal} = 94.08\ \frac{W}{m^2.kg.℃}$, *and* $\overline{\alpha}_{ETSC,normal} = 5.22\ \frac{W}{m^2.kg.℃}$. By incorporating one CPC in the system, the value of α decreased by 9.25, and α reached *84.83* $\frac{W}{m^2.kg.℃}$ i.e., $\alpha_{SWH,CPC} = 84.83\ \frac{W}{m^2.kg.℃}$. In addition, the energy flux enhancement by CPC is achieved from the difference between the total energy flux in the conventional device and the system with one concentrator as follows: $\alpha_{CPC} = \alpha_{SWH,normal} -$

$\alpha_{SWH,CPC} = 94.08 - 84.83 = 9.25 \frac{W}{m^2.kg.°C}$. Also, for the CPC system, the average energy flux of an absorber tube with a concentrator is: $\overline{\alpha}_{ETSC,CPC} = 5.22 + 9.25 = 14.47 \frac{W}{m^2.kg.°C}$. An important outcome is that the integration of CPC and ETSC resulted in a system that is 2.77 times more efficient than a conventional system. In other words, the SWH with 18 ETSC absorber tubes and SWH with 7 ETSC equipped with CPC demonstrated similar performance.

4. CONCLUSIONS

In conclusion, the application of Solar Water Heaters (SWH) with Evacuated Tube Solar Collectors (ETSC) absorbers has become commonplace. However, in this type of SWH, the full capacity of ETSC is not fully utilized, as half of the ETSC is not always exposed to direct sunlight. To overcome this limitation, various concentrators are employed. This research aimed to compare the performance of a Compound Parabolic Concentrator (CPC) and ETSC under a specific area ratio. The overall system performance, as well as the performance of an individual ETSC, were monitored alongside the atmospheric conditions. The same system with the concentrator was tested under certain weather conditions the following day. As a novel comparison tool, the performance of SWH has been evaluated by introducing the new coefficient "α" as the absorption rate of solar energy required to increase the temperature of 1 kg of working fluid by 1°C in a solar water heater. After installing the concentrator, α was reduced to 9.25 $\frac{W}{m^2.kg.°C}$. This can be a suitable characteristic to compare SWHs of different capacities, geometries, and conditions. Wherever "α" is smaller, the overall energy performance of SWH would be higher.

The results obtained from this study are as follows:

(a) Under the same weather conditions, the water temperature in the tank increased by 2.3 ºC at the end of the data collection period after installing the concentrator compared to the normal state.

(b) According to the energy efficiency changes graph, ETSC with a concentrator experiences less loss than ETSC in normal mode. Also, under conditions where the average radiation is about 750 $\frac{W}{m^2}$, the average efficiency of the system with the concentrator was 2.8% higher than the efficiency of the conventional device, reaching 74.7% in the highest state, whereas the highest efficiency of the conventional system was 72.9%.

(c) It was observed that the average α was reduced by 9.25 $\frac{W}{m^2.kg.°C}$ after installing the concentrator.

(d) From the comparison of α in the two states, it can be concluded that an ETSC equipped with a CPC became 2.77 times more efficient than the conventional system. In other words, a SWH with 18 ETSC and a SWH with 7 ETSC equipped with the CPC had the same performance.

Future work on the present study involves investigating this system with a sun tracker on the concentrator, as well as a time-dependent dynamic modeling of the system with CPC, and using machine learning to estimate the energy storage changes in the storage tank.

5. ACKNOWLEDGEMENT

This work was supported by the Materials and Energy Research Center (MERC) under Grant No. 571398056.

NOMENCLATURE

Abbreviations

SWH	Solar water heater
ETSC	Evacuated tube solar collector
CPC	Central parabolic concentrator
IEA	International energy agency
NEPCMs	Nano-enhanced phase change materials
EBIETC	Embedded building integrated solar evacuated tube collector
ETSC-IC	Evacuated tube solar collector with inner concentrating
M-CPC	Multi-section compound parabolic concentrator

Symbols

G_s	Solar irradiation (W/m^2)
T	Temperature (°C)
d	Free space under ETSC (m)
r	Radius of cycle (m)
R	Length of arc (m)
F	Focal length (m)
v	Wind speed (m/s)
Q	Heat flux (W)
Nu	Nusselt number
C_o	Correction factor of Nu
Pr	Prandtl number
g	gravitational constant (m/s^2)
C_p	Specific heat capacity (kJ/(kg.°C))
m	Mass (kg)
A	Area (m^2)

Greek letters

α	Energy absorption rate
φ	Angle of arc
λ	Thermal conductivity W/(m.°C)
β	Collector inclination angle (°)
η	Efficiency
ϑ	Declination angle
ν	Kinematic viscosity (m^2/s)
γ	Specific weight (N/m^3)

Subscripts

a	Ambient
t	Storage tank
h	Hot water exits from thermosiphon cycle
c	Cold water enters in thermosiphon cycle
w	Working fluid
s	Sun
gl	Glass
T_{io}	Outer temperature of the inner tube
T_{ii}	Internal temperature of the inner tube
D_{io}	Outer diameter of the inner tube
D_{ii}	Internal diameter of the inner tube

Acronyms

normal	Normal system without any change
CPC	System with installed CPC
use	Useful
st	At the beginning of the period
e	At the end of the period
abs	Absorber
in	Total input
en	Energy
Ex	Exergy
DW	Durbin Watson test

REFERENCES

1. Budihardjo I, Morrison GL. (2009). Performance of water-in-glass evacuated tube solar water heaters. Solar Energy. 83(1):49-56. https://doi.org/10.1016/j.solener.2008.06.010

2. Chai S, Yao J, Liang J-D, Chiang Y-C, Zhao Y, Chen S-L, et al. (2021). Heat transfer analysis and thermal performance investigation on an evacuated tube solar collector with inner concentrating by reflective coating. Solar Energy. 220:175-86. https://doi.org/10.1016/j.solener.2021.03.048

3. Chen F, Liu Y. (2022). Model construction and performance investigation of multi-section compound parabolic concentrator with solar vacuum tube. Energy. 250:123887. https://doi.org/10.1016/j.energy.2022.123887

4. Chen X, Yang X, Li M. (2022). Combining horizontal evacuated tubes with booster mirror reflector to achieve seasonal reverse output: Technical and experimental investigation. Renewable Energy. 188:450-64. https://doi.org/10.1016/j.renene.2022.02.041

5. Chen F, Xia E-t, Bie Y. (2019). Comparative investigation on photo-thermal performance of both compound parabolic concentrator and ordinary all-glass evacuated tube absorbers: An incorporated experimental and theoretical study. Solar Energy. 184:539-52. https://doi.org/10.1016/j.solener.2019.04.036

6. Deng C, Chen F. (2020). Preliminary investigation on photo-thermal performance of a novel embedded building integrated solar evacuated tube collector with compound parabolic concentrator. Energy. 202:117706. https://doi.org/10.1016/j.energy.2020.117706

7. Durbin, J., Watson, G. S. (1950). Testing for Serial Correlation in Least Squares Regression, I, Biometrika. 37 (3–4), 409–428. https://doi.org/10.1093/biomet/37.3-4.409.

8. Durbin, J.; Watson, G. S. (1971). Testing for serial correlation in least squares regression, III". Biometrika. 58 (1), 1–19. https://doi.org/10.2307/2334313.

9. Fathabadi H. (2020). Impact of utilizing reflector, single-axis and two-axis sun trackers on the performance of an evacuated tube solar collector. International Journal of Green Energy. 17(12):742-755. https://doi.org/10.1080/15435075.2020.1798766

10. Hossein Ghadamian, Meisam Moghadasi, Mojtaba Baghban yousefkhani, Masoumeh Javaheri, Abouzar Massoudi, Hajar Amiria (2024). Experimental investigation on a novel empirical parameter for simultaneous analysis of the temperature and concentration effects on fuel utilization coefficient of direct ethanol fuel cell, Renewable Energy, Volume 224, 120132, ISSN 0960-1481, https://doi.org/10.1016/j.renene.2024.120132.

11. Ismail KAR, Teles MPR, Lino FAM. (2021). Comparative analysis of eccentric evacuated tube solar collector with circular and rectangular absorber working with nanofluid. Cleaner Engineering and Technology. 3:100105. https://doi.org/10.1016/j.clet.2021.100105

12. King, M.L., 1992. Introduction to Durbin and Watson (1950, 1951) Testing for Serial Correlation in Least Squares Regression, Springe: I, II, Breakthroughs in Statistics. https://doi.org/10.1007/978-1-4612-4380-9_19.

13. Kumar PM, Mylsamy K. (2020). A comprehensive study on thermal storage characteristics of nano-CeO_2 embedded phase change material and its influence on the performance of evacuated tube solar water heater. Renewable Energy. 162:662-676. https://doi.org/10.1016/j.renene.2020.08.122

14. Li Q, Gao W, Lin W, Liu T, Zhang Y, Ding X, et al. (2020). Experiment and simulation study on convective heat transfer of all-glass evacuated tube solar collector. Renewable Energy. 152:1129-1139. https://doi.org/10.1016/j.renene.2020.01.089

15. L. Seidabadi, H. Ghadamian, M. Aminy, M. Moghadasi & S. Ghahremanian, (2022). Simulation and experimental investigation of an organic phase change material-based air-cooling system for industrial applications in the hot climate, Energy Sources, Part A: Recovery, Utilization, and Environmental Effects, 44:1, 796-816. https://doi.org/10.1080/15567036.2022.2050965.

16. Mevada D, Panchal H, ElDinBastawissi HA, Elkelawy M, Sadashivuni K, Ponnamma D, et al. (2022). Applications of evacuated tubes collector to harness the solar energy: a review. International Journal of Ambient Energy. 43(1):344-61. https://doi.org/10.1080/01430750.2019.1636886

17. Milani D, Abbas A. (2016). Multiscale modeling and performance analysis of evacuated tube collectors for solar water heaters using diffuse flat reflector. Renewable Energy. 86:360-374. https://doi.org/10.1016/j.renene.2015.08.013

18. Moghadasi, M., Ghadamian, H., Moghadasi, M., Seidabadi, L. (2023). Prediction of outlet air characteristics and thermal performance of a symmetrical solar air heater via machine learning to develop a model-based operational control scheme—an experimental study. Environ Sci Pollut Res 30, 27175–27190. https://doi.org/10.1007/s11356-022-24169-0

19. Pourbafrani, M., Ghadamian, H., Moghadasi, M. & Mardani, M. (2023) Design, Fabrication, and Experimental Study of a Low-cost and Accurate Weather Station Using a Microcontroller System. Journal of Renewable Energy and Environment (JREE), 10(4), 35-43. https://doi.org/10.30501/JREE.2023.383796.1551.

20. M. Moghadasi, N. Izadyar, A. Moghadasi, H. Ghadamian. (2021). Applying machine learning techniques to implement the technical requirements of energy management systems in accordance with iso 50001: 2018, an industrial case study, Energy Sources, Part A: Recovery, Utilization, and Environmental Effects, 1–18. https://doi.org/10.1080/15567036.2021.2011989

21. M. Moghadasi, H. Ghadamian, M. Khodsiani, M. Pourbafrani, (2022). A comprehensive experimental investigation and dynamic energy modeling of a highly efficient solar air heater with octagonal geometry, Solar Energy, Volume 242, Pages 298-311, ISSN 0038-092X, https://doi.org/10.1016/j.solener.2022.07.030

22. Qiu S, Ruth M, Ghosh S. Evacuated tube collectors: (2015). A notable driver behind the solar water heater industry in China. Renewable and Sustainable Energy Reviews. https://doi.org/47:580-8.10.1016/j.rser.2015.03.067

23. Sadeghi G, Safarzadeh H, Ameri M. (2019). Experimental and numerical investigations on performance of evacuated tube solar collectors with parabolic concentrator, applying synthesized Cu_2O/distilled water nanofluid. Energy for Sustainable Development. 48:88-106. https://doi.org/10.1016/j.esd.2018.10.008

24. Sasikumar SB, Santhanam H, Noor MM, Devasenan M, Ali HM. (2020). Experimental investigation of parallel type -evacuated tube solar collector using nanofluids. Energy Sources, Part A: Recovery, Utilization, and Environmental Effects. 1-13. https://doi.org/10.1080/15567036.2020.1829201

25. Shoaib Khanmohammadi, Mohammad Mehdi Baseri, Pouria Ahmadi, Abdullah A.A.A. Al-Rashed, Masoud Afrand, (2020). Proposal of a novel integrated ocean thermal energy conversion system with flat plate solar collectors and thermoelectric generators: Energy, exergy and environmental analyses, Journal of Cleaner Production, Volume 256, 120600, ISSN 0959-6526, https://doi.org/10.1016/j.jclepro.2020.120600.

26. Teles MdPR, Ismail KAR, Arabkoohsar A. (2019). A new version of a low concentration evacuated tube solar collector: Optical and thermal investigation. Solar Energy. 180:324-39. https://doi.org/10.1016/j.solener.2019.01.039

27. Wang Q, Shen B, Huang J, Yang H, Pei G, Yang H. (2021). A spectral self-regulating parabolic trough solar receiver integrated with vanadium dioxide-based thermochromic coating. Applied Energy. 285:116453. https://doi.org/10.1016/j.apenergy.2021.116453

28. Xia E-T, Chen F. (2020). Analyzing thermal properties of solar evacuated tube arrays coupled with mini-compound parabolic concentrator. Renewable Energy. 153:155-67. https://doi.org/10.1016/j.renene.2020.02.011

29. Yousef FathiAlmas, Hossein Ghadamian, Mohammad Aminy, Meisam Moghadasi, Hajar Amirian, Siamak Hoseinzadeh, Davide Astiaso Garcia, (2023). Thermo-economic analysis, energy modeling and reconstructing of components of a single effect solar–absorption lithium bromide chiller for energy performance enhancement, Energy and Buildings, Volume 285, 112894, ISSN 0378-7788, https://doi.org/10.1016/j.enbuild.2023.112894.